Experimental Aspects of Ultra Cold Gases:

A Work Term Summary

by
Paul Martin Lebel

Supervisor: Dr. Kirk Madison
Quantum Degenerate Gas Lab

Submitted to: Nicole Benda
APSC 310

The University of British Columbia
January 19, 2007

Abstract

This paper is an expository document describing numerous experimental aspects of ultra cold atoms, based entirely on the work completed in the current term of May-August 2006. A ^{87}Rb MAT (Miniature Atom Trap) has been built from start to finish, with the exception of its laser stabilization scheme. To that end a slave laser amplifier system, magnetic coils, and an UHV system have been assembled. I present a few basic loading rate measurements taken by myself and Dr. James Booth from BCIT, who was instrumental in the conception and rapid success of the experiment. Several magnetic coils and a pair of high voltage electrodes have been designed as part of a heteronuclear Feshbach resonance experiment in the same lab. For these I present a short description, specifications, and several photographs. Finally, a numerical simulation has been written to predict the performance of a magnetic waveguide as low-pass velocity filter.

Table of Contents

Appendices

List of Figures

Glossary

Acousto-Optical Modulator (AOM)	A frequency shifting device making use of Doppler-shifted Bragg Diffraction. Acoustic waves propagating through a quartz crystal create a traveling density modulation, causing an incident monochromatic light field to split into angularly separated diffraction orders of different frequency.
Anodic Bonding	Anodic bonding is a chemical reaction induced by a strong DC electric field. In context, Jim Booth hopes to seal a vacuum chamber by anodically bonding a silicon wafer to the end of a glass cell. In this case, sodium ions present near the glass surface are repelled away by the electric field, rendering the surface highly reactive to the nearby silicon.
Baking	Baking is when a vacuum system is brought to elevated temperatures upwards of 400°C to burn off gasses dissolved within the container walls. The released gasses temporarily elevate the pressure in the system until they are pumped out and the rate of outgassing decreases to a level lower than before baking. When the system is cooled, its pressure can be several orders of magnitude lower than before the bake.
Bose-Einstein Condensate (BEC)	A degenerate state of matter predicted by Albert Einstein and Satyendra Bose in 1924. A BEC behaves as a coherent matter wave, much like a laser is to an incandescent bulb.

Chip Trap	A small substrate etched with current carrying wires above which cold atoms are held by the Zeeman force of the magnetic trap. Because of their small size, chip traps can achieve extraordinarily high field gradients.
Feshbach resonance	A vibrational resonance occurring when the kinetic energy of two colliding atoms equals the bound state energy of the diatomic molecule that could result from a collision. The position of the resonance can be tuned by the strength of an external magnetic field, whose measurement in Li–Rb systems is one of the immediate goals of the QDG lab.
Helmholtz pair	A pair of circular magnetic coils having radius equal to their separation distance. The field from a Helmholtz pair maximizes flatness in the geometric center, being uniform to $\bigcirc\{z^4\}$ in both the axial and radial directions. An Anti-Helmholtz pair is the same thing but with current reversed in one coil, and has zero field in the center and linearly increasing field in all directions originating from the center. Most MOTs use Anti-Helmholtz coils to produce their quadrupolar gradients.
Magneto-Optical Trap (MOT)	The most commonly used technique for producing ultra-cold atoms, developed by `AT&T` Bell labs in 1987. The trap uses velocity selective radiation pressure in combination with a spatially dependant zeeman effect to slow and confine atoms into an ultra-cold cloud.
Master Laser Table	The centralized optical table at QDG lab, supporting all five master diode lasers and associated control electronics and frequency stabilizing optics. Light from the master table is piped to all individual experiments via single-mode fiber optic cables, where it is either amplified or used directly.

Miniature Atom Trap (MAT)	The title of Dr. Booth's trap miniaturization/commercialization experiment in collaboration with UBC. Potential confusion: The MAT has a small MOT, but will be more than just a MOT. See chapter 3 for details.
Mirror MOT	A MOT that is formed near the surface of a mirror. The incident and reflected light fields of two counter-propagating laser beams aligned at 45° to a mirror provide trapping force, as opposed to using retro-reflecting mirrors in the far-field. A mirror MOT also has a third (retro-reflected) beam which propagates tangent to the plane of the mirror, and exerts confinement force along its axis.
Optical Molasses	A region created by the intersection of red-detuned laser beams. Classically, the field exerts a viscous drag force on an atom passing through the region.
Photodesorption	A method of releasing a flux of atoms previously bound to a surface, by using a pulse of visible or ultraviolet light.
Non-Evaporable Getter(NEG)	A type of vacuum pump which uses a chemically reactive filter to remove contaminants from a vacuum system. NEG pumps can only pump a limited range of elements.
Quantum Degenerate Gas Lab (QDG)	UBC's ultra-cold physics lab, led by Dr. Kirk Madison. See the research website at www.phas.ubc.ca/~qdg/
Skimmer[5]	A laser-free slow atom source. Its name is derived from the principle of operation: the device is a low pass velocity skimmer for weak field seeking atoms. The lower portion of the Maxwell-Boltzmann distribution is allowed to pass through an evacuated tube and onwards into a trapping chamber.

Sweep	A frequency sweep (in the form of a sawtooth function) is often applied to the master lasers by modulating a combination of the current and diffraction grating positions. The frequency sweep is useful for the spectroscopic analysis that is required prior to locking. One may set the sweep width as well as frequency.
Ultra High Vacuum (UHV)	A gas-filled container is said to have UHV conditions if the total pressure inside is less than 10^{-8} torr.

Acknowledgements

I would like to thank everyone at the QDG* lab for giving me this opportunity to work on such exciting projects. As an undergraduate, I feel extremely privileged to have been included in the detailed planning and execution of the Feshbach* and MAT* experiments, as opposed to being given one narrow-minded task. More specifically, my thanks go to Tao Kong for helping me with F90, Swati Singh,Janelle Van Dongen, and Keith Ladouceur for perpetually helping me with everything from optics and electronics to lending me pizza money, Dr. Bruce Klappauf for his incredible ability to solve almost any problem (see the figure on aligning a Double pass AOM), Dr. James Booth for sharing his valuable knowledge and experience as a mentor on the MAT experiment, and of course Dr. Kirk Madison for his leadership, experience, generosity, and enthusiasm as a supervisor.

Chapter 1

Introduction

This document describes in detail the work I have completed over the eight month term spanning May-December 2006, sandwiched between my third and fourth years of undergrad. It encompasses a number of projects all related to the experimental side of laser cooling and trapping alkali metals, and can be broken down as follows:

1. MAT* experiment in collaboration with Dr. James Booth
2. Mechanical and Magnetic field design for the Feshbach resonance* experiment
3. Cold Atom Source design
4. Mechanical and Magnetic field design for the Photo-Association experiment in David Jones' Ultrastable Femtosecond optics lab

Although they are separate experiments, all of the above share a common optical frequency stabilization scheme: the master laser table*. The generation of frequency-stabilized laser light is essential to any process involving the control of atomic motion by radiation pressure, but it is also one of the more technically-challenging tasks. As such, the process is done once and for all on the master table and the light is distributed wherever it is needed, by means of optical fiber splitters and single-mode fiber optic cables. This paper does not describe the frequency locking process in detail, but it is crucial to all the experiments and ensuring the masters are locked is an ongoing task.
The second section of this report covers a small amount of theory and some of the basic infrastructure of the lab, as background to the other experimental systems. The goal of lab's infrastructure is to automate entire experiments through an organized hierarchy of computer controlled devices. Presently, the hardware is nearly all in place but the control software is still under development. The third section provides a detailed description of the MAT experiment, some preliminary results, and future work. Written

in the fourth section is my work on the Feshbach experiment, which focusses on mechanical and magnetic field design, including several solidworks and Matlab models. Finally, section five will cover a literature search on cold atom sources as well as a numerical simulation of atomic trajectories in a magnetic waveguide, whose intent is to model the performance of a laser-free slow atom source (skimmer*) for potential use in any of the above experiments. My contribution to the Laboratory of Ultrastable Femtosecond optics is worth mentioning only in that two of my magnetic coil designs for the Feshbach experiment have been exactly duplicated for their use; I did not contribute any work unique to that lab.

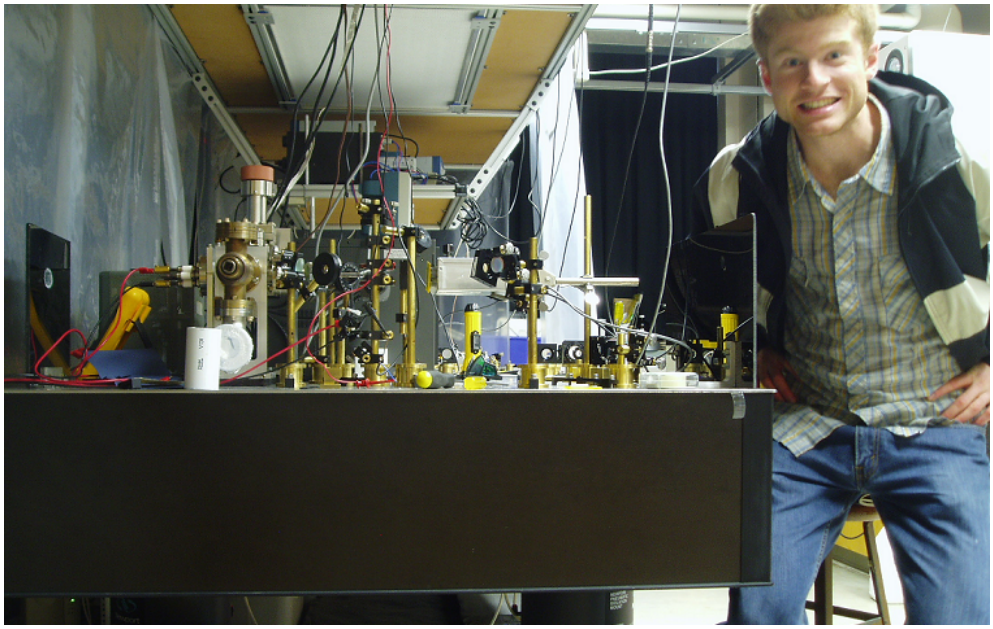

Figure 1.1: A grinning undergrad student about to hit the bouldering gym.

Chapter 2

Experimental Background

This section is not exactly a chapter unto its own, but rather a small collection of information which is needed as background to understand the experimental systems described in the other chapters. I will omit the theory of how a MOT works, as there are a multitude of other resources available, including a description in my previous report[9]. Suffice it to say that a MOT requires near-UHV conditions, an atomic source dispensing the species of interest, a quadrupole magnetic field, and two specific frequencies of light–cooling light and repump light. Cooling light must be incident on the magnetic field minimum from all directions, and circularly polarized with one helicity in the radial plane (radial with respect to the magnetic coils) and the other helicity in the axial direction. It is not mandatory that repump light come from any particular direction; only its presence is required.

2.0.1 The Laser System

The frequency-stabilized light is produced by an array of master diode lasers, all of which rest on an isolated platform above the optical locking setup on the table below. This light can then be amplified in multiple stages by more diode lasers ('slave' lasers) through injection locking. Injection-locked slave lasers can be conveniently placed wherever they are needed, thanks to the wonders of fiber-optic cables carrying the master light to the slaves. Additionally, the slaves do not require the locking electronics or environmental isolation that is required by the masters.

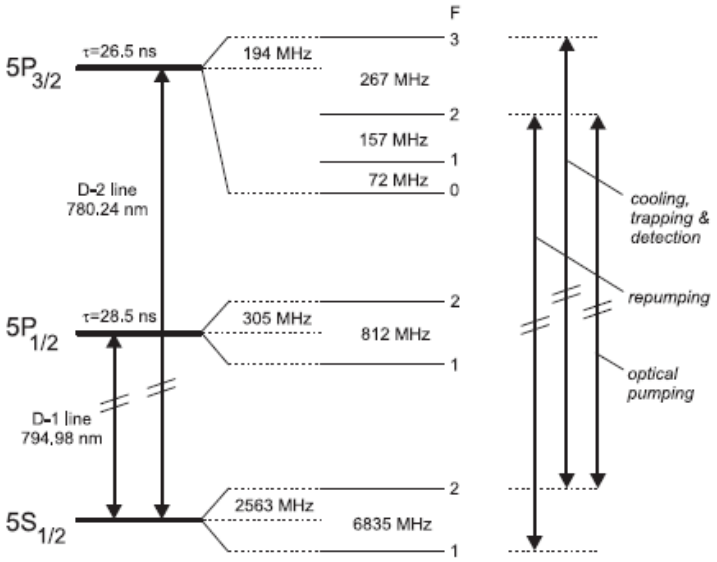

Figure 2.1: [4]The hyperfine structure of ^{87}Rb. All of our work with ^{87}Rb makes use of the D2 line at 780.24nm. MOT light for cooling and trapping is tuned just red of the $|F = 2 \rightarrow 3' >$ transition, whereas repump light is tuned directly to the $|F = 1 \rightarrow 2' >$ transition. Note that the frequency splittings given in MHz are far smaller than the 14.74nm separating the D1 and D2 lines. The Acousto-optical modulators are used to shift frequency anywhere between 60-200MHz, depending on the make/model and whether it is aligned for single or double pass.

The master lasers produce light in such a way that makes it possible to shift its frequency and amplify it in a modular fashion. Using an innovative saturated absorption technique, the master lasers are locked to a frequency that is some 160MHz below the cooling transition $|F = 2 \rightarrow 3' >$ on the D2 line of ^{87}Rb. Once this light is delivered to the MAT table, it can be shifted or modulated by an AOM, which is used for optimizing or modulating the frequency detuning as well as suddenly disrupting the light field; all of which may be controlled electronically via digital and FM inputs to the AOM driver.

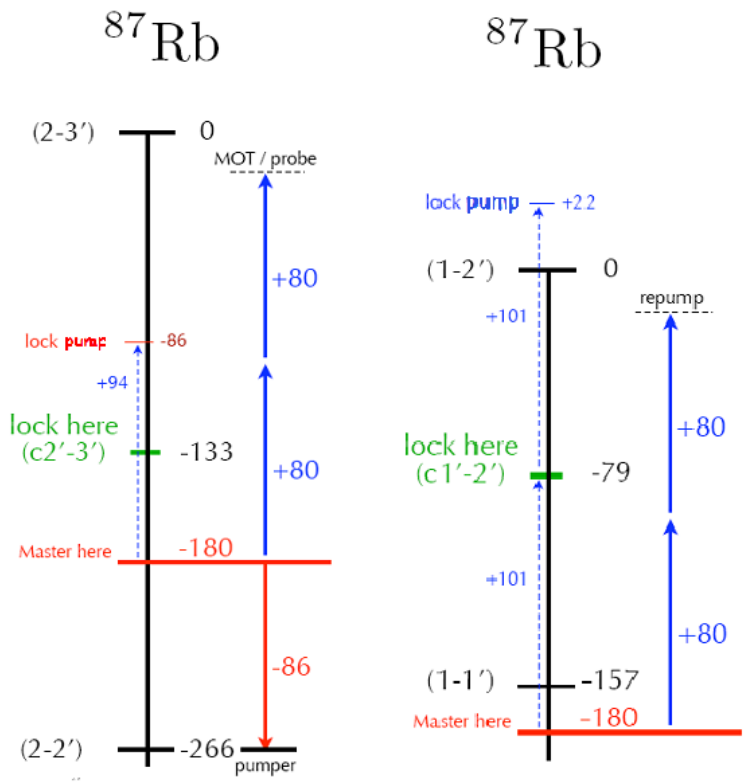

Figure 2.2: The experimental reality of locking, amplifying, then frequency shifting laser light for cooling and trapping. One master is used for cooling light (left) and another for repump light (right). 'Lock here' points to the spectroscopic feature which is being used for locking–the two crossover transitions shown in green. These features are not the frequencies of the masters nor in fact any of the light, but they are intermediate frequencies which arise as a result of a certain velocity class of atoms interacting simultaneously with a master's light and its counter-propagating pump laser in saturated absorption. As such, when one locks to the crossover transition, the master laser is forced to be $\frac{\delta}{2}MHz$ red of this frequency, where δ is the frequency difference between the pump and the master. It is the master light which is delivered to the other experiments ('Master here'). The blue $+80MHz$ arrows indicate the double-pass AOM shifting done afterwards on the MAT table.

2.0.2 UHV System

The UHV systems are pumped down with a mobile pumping station which includes a roughing pump, a turbo pump, a residual gas analyzer, thermocouple sensors, and some other diagnostic tools. This station connects to any given system (in our case, the MAT ion pump, NEG pump, Rb dispenser and glass cell) that is mounted on standard 2.75" conflat vacuum flanges. The system is pumped down by the mobile station and then repeatedly baked* until the pressure drops to a level where it is safe to turn on the ion pump and/or NEG pump. This same station will be used to pump down the Feshbach system, located across the lab from the MAT table.

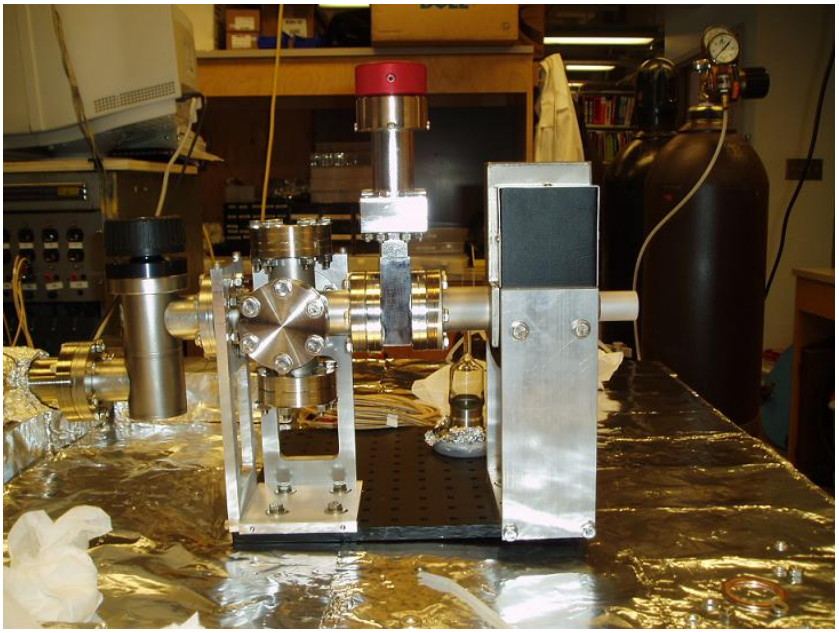

Figure 2.3: The vacuum system for the MAT, before installation on the optical table. At this stage, rough pumping on the cell was about to be tested, and the subsequent discovery of a leaky cell. The cell was repaired with VacSeal and is now in use.

Chapter 3

MAT Experiment

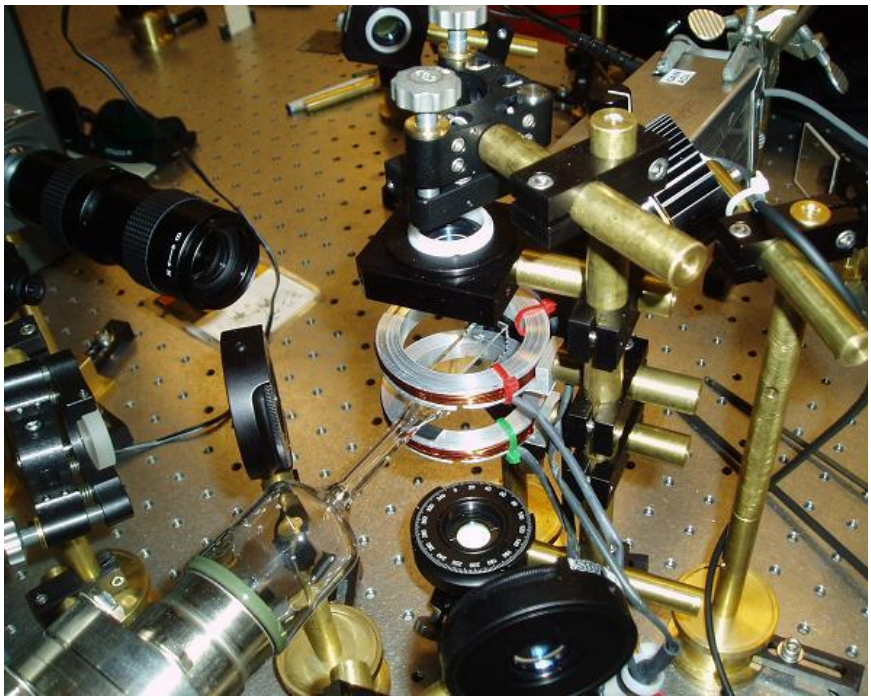

Figure 3.1: The vacuum cell, magnetic coils, and surrounding MOT optics of the MAT experiment. Trapping occurs at the intersection of six beams and the magnetic field zero in the center of the cell.

The Miniature Atom Trap (MAT) experiment is an exciting new collaboration between Dr. Kirk Madison and Dr. James Booth from BCIT. It is located at the QDG lab, and therefore makes use of the existing infrastructure such as master light for cooling and repump, temperature and current controllers for its slave amplifier, optical table space, and much more. James Booth and I began work on the MAT experiment began in early September,

and since that time we have made a great deal of progress:

Assembly of a diode laser for use as a slave amplifier	September 4^{th}
First signs of injection locking	September 25^{th}
Upper limit on the free running slave's spectral linewidth determined	October 16^{th}
Saturated absorption spectroscopy measurements performed with the MAT slave	November 16^{th}
Vacuum system operational	December 6^{th}
A ^{87}Rb MOT of estimated size 10^7	**December 12^{th}**
Confirmation of UV induced photo-desorption*	December 14^{th}
Preliminary measurements of magnetic trapping in a pure quadrupole	December 16^{th}
Measurement of MOT loading rates under various experimental parameters: magnetic gradient strength, dispenser current, light polarization type, and laser detuning.	December 12-17

3.1 Goals

The purpose of the MAT experiment is to investigate the possibility of commercializing cold atom traps, to the end of making them more accessible for general areas of research. Ultra-cold atoms are currently produced in the context of university research labs with considerable resources and labspace available to develop the necessary apparatus and control systems. If this factor can be minimized to the point where a vacuum/dispenser system can be made portable, it would be a big step towards making cold atom traps readily available to researchers in other fields.
The most likely uses for ultra cold atoms is in making advanced sensors: atomic clouds have proven to be highly sensitive to environmental perturbations, making them ideal candidates for many types of sensors. Magnetometers, inertial sensors, and GPS clocks have already been demonstrated

in laboratory settings. The MAT experiment will hopefully become a 'test platform' for these types of cold atom sensors [1].
The immediate goals are to investigate how to minimize the cost and complexity of the UHV* system. Typically, a cold atom trap requires multiple stages of pumping in order to achieve the necessary vacuum quality of around 10^{-9} torr for a rudimentary MOT, and roughly 10^{-10} torr to evaporate to degeneracy. In the qdg lab, this is done with a portable pumping station equipped with a roughing pump and a turbo pump. After these pumps evacuate a chamber to their limit, they are closed off and then an ion pump and a NEG* pump are connected to the system and turned on. The ion and NEG pumps, combined with numerous bakings*, can achieve pressures as low as 10^{-10} or sometimes lower, depending on the total rate of outgassing in the system.
The MAT will test the quality of vacuum that is maintainable by using only a NEG, as opposed to using both an ion pump and a NEG. This technique requires an initial use of the ion pump, but would be disconnected from it once the initial pumping is complete. The advantage of only using a NEG pump is its minimal cost, size, and power requirements. Since the device is simply a temperature controlled chemical reactor, its only requirement is a DC power supply capable of a few amperes. In addition to testing the limits of a minimal pumping system, the MAT experiment also attempts to minimize the actual vacuum quality that is required for trapping.
The MAT experiment will hopefully cool atoms to degeneracy in a chip trap* formed by a silicon substrate anodically bonded* to the end of a glass cell. The chip trap takes advantage of its small size to achieve high magnetic field gradients, since in general the gradient strength scales like $\frac{1}{a^2}$, where a is the length scale of the trap. For example, take the axial component of the field produced by an anti-Helmholtz* coil pair; the simplest way of producing three-dimensional confinement in a magnetic trap:[1]

$$B_z = \frac{24}{25}\sqrt{\frac{4}{5}}\frac{\mu_o N I}{a^2}z - \frac{72}{125}\sqrt{\frac{4}{5}}\frac{\mu_o N I}{a^4}z^3 + \bigcirc\{\frac{z^5}{a^5}\} \tag{3.1}$$

Where a is the radius of each coil as well as their separation. Taking the derivative with respect to z and then making the approximation that $z \ll a$ gives an approximation for the field gradient:

$$B_z{}' = \frac{24}{25}\sqrt{\frac{4}{5}}\frac{\mu_o N I}{a^2} \tag{3.2}$$

Which shows the inverse square dependance as stated above. Steep magnetic traps (those with high gradients) have a high rate of atomic oscillation and

increased density, thereby enhancing the collision rate between atoms[15]. This property shortens the timescale required for evaporative cooling and production of a BEC, reducing the total number of collisions with the high energy background gas. As a result, the requirement for vacuum quality may be loosened in the case of a steeper magnetic trap. The small size of the MAT takes advantage of this gradient scaling property, as well as an overall reduction in cost of materials.

3.2 System Overview

Presently, the MAT experiment consists of a slave laser amplifier, a double-pass AOM*, a saturated absorption spectroscopy diagnostic, MOT optics, and an UHV system. These elements are all described individually below, but not to be forgotten is the master laser table, which provides single mode frequency-locked laser light for both the 'cooling' and 'repump' transitions. Functionality of the master laser system is crucial to the entire MAT experiment. Although presently the system is nearly in a state of robust operation, the master lasers require frequent tuning and adjustments to achieve locking; a constant reminder of the inherent complexity of the experiment.

3.2.1 Slave Laser Amplification

The slave laser amplifier is a current-controlled diode laser in a temperature-controlled aluminum case. The individual parts for this laser were available in the lab and required assembly and the soldering of a small protection circuit. Once assembly was complete, the laser was clamped in place on the optical table and its cables extended over to the central control manifold located next to the master laser table. In the present configuration, the amplifier is only being used to amplify *cooling* light, not repump light, which is mixed into the cooling beam directly from an optical fiber.

The sole purpose of the slave laser is to amplify incoming single mode, narrow linewidth light from the master laser table. In this situation, it is critically important to minimize optical feedback from any other free-running modes the slave happens to produce. Hence, the first optical component (other than two mirrors for alignment purposes) in the path of the slave laser is an optical isolator. The isolator allows the slave's linearly polarized to pass through with 85% efficiency in one direction, but heavily attenuates all light travelling the other direction. The isolator also feature an optical input port, which protrudes at a different angle than the main port and allows light polarized orthogonal to the slave's light to couple into its path

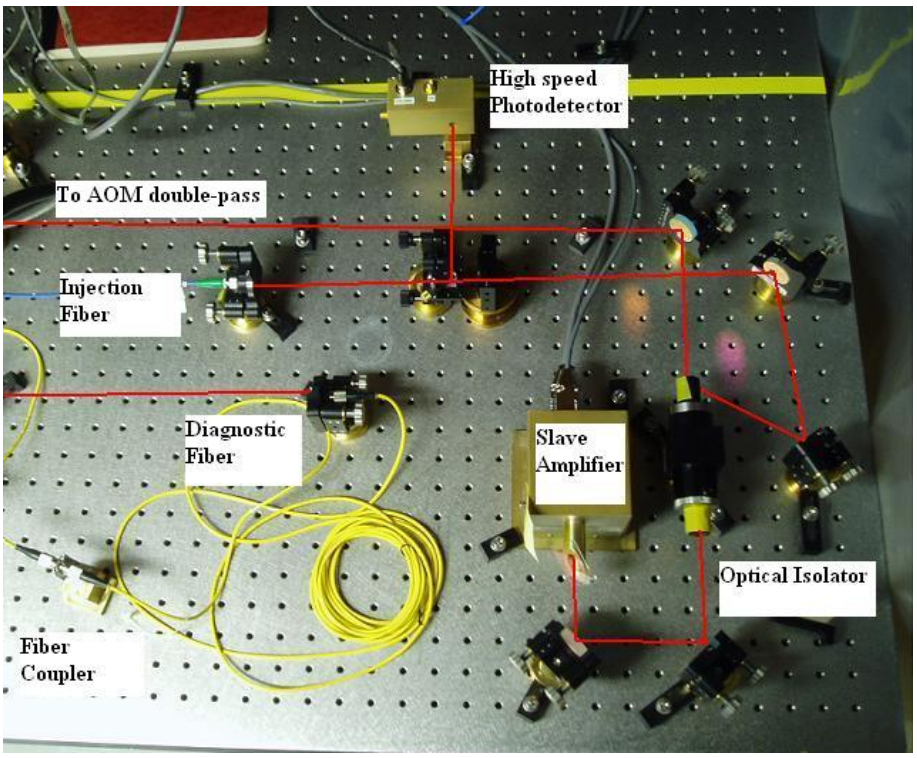

Figure 3.2: The slave amplifier system for the MAT experiment. Single mode light tuned 180MHz below the $|F = 2 \rightarrow 3' >$ transition of ^{87}Rb coming from the master laser table is collimated from the injection fiber. This light is coupled back into the slave's beam path through the input port on an optical isolator, which otherwise prevents any optical feedback to the slave. Output from the slave passes through the isolator's main port and onwards to the double-pass AOM. Also visible is a portion of the beam coupled back into a yellow multimode fiber for diagnostic.

back towards the source. We therefore use the optical input port to send master light into the slave laser diode, where it acts as optical feedback to dominate the gain medium and induce amplification.
The amplified light emerges from the isolator and is directed into the double-pass AOM, where it is frequency-shifted to some amount δ(called the detuning) below the $|F = 2 \rightarrow 3' >$ transition. The AOM can operate in the range between ±60-100MHz, and therefore a double-pass can shift anywhere between ±120-200MHz. Typically we run the AOM at around 80MHz, shifting the master light from -180MHz up to -20MHz; a detuning that is optimal for cooling[13].
Alignment of the double-pass is complicated by the fact that:

1. The AOM operates most efficiently when the beam is focused on the crystal itself, requiring either two lenses or one lens which focuses the beam onto a mirror that is placed as close as possible to the device.

2. The AOM produces several different orders of diffraction, the correct one of which must be chosen, isolated, and re-directed back into the device.

3. In order to separate the outgoing beam from the incoming beam, a polarization-dependent beamsplitting cube must be used.

4. The polarization must therefore undergo a 90° rotation at some point in the double pass.

5. The diffracted light emerges at an angle which is proportional to the frequency shift, rendering an alignment job useless if the shift frequency is modified. Using a spherical mirror to reflect the re-directed light alleviates this problem.

To accomplish all this, we pass horizontally polarized light consecutively through a cube, a focusing lens, an aperture, the AOM, a quarter wave plate (QWP), and then a spherical mirror. When the singly-diffracted beam reaches the spherical mirror, it retraces its path back through the AOM, but now its polarization is rotated to the vertical axis, having passed twice through a quarter wave plate. The vertically polarized beam retraces the same path up to the cube, where it is now reflected instead of transmitted.

The shifted light propagates down to the other side of the table where it is expanded with a pair of lenses by a factor of 2.5. The beam is split into three–one for each axis–and directed towards the vacuum cell. Each beam passes through a QWP, the vacuum cell, another QWP, and then is

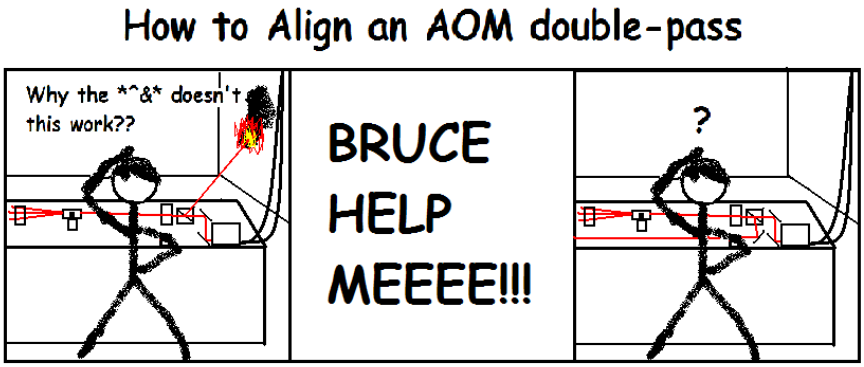

Figure 3.3: How to align an AOM double-pass

reflected directly back from a planar mirror. This technique is called retro-reflection, and it has the same effect as passing six different beams from all the cartesian axes. The purpose of the QWP's is to make the polarization of the light circular as it propagates through the cell. Moreover, the reflected beams have the same helicity (RCP or LCP) as the original incoming beams because the second QWP converts the light to linear and then back to the same circular polarization as was incident.
The repump light is mixed with the cooling light on the same cube as is used for the double-pass and is not frequency shifted. The repump light propagates along with the cooling light and is expanded and split as described above.

Injection Diagnostics

A multitude of diagnostic tools are available to confirm injection locking. The following checks can be performed on the output of the slave amplifier, however unfortunately, none of them individually confirms absolute injection locking.

Atomic fluorescence The output of the slave is directed into a Rb vapor cell. With the use of an IR viewer, one may see a beam of fluorescing atoms if any optical power coincides with one of the Doppler-broadened absorption peaks.

Optical Spectrum Analyzer This can be used to identify large shifts in frequency that are caused by blocking/unblocking the master light,

whether it be due to injection locking or alteration of material properties caused by the incident light.

Fabry-Perot cavity A Fabry-Perot cavity transmits resonant modes, which are visible as a photodiode voltage on an oscilloscope. If the resonant frequencies are actively modulated by a piezo crystal on a timescale much faster than the sweep* frequency of the master laser, one can observe the sweeping mode as a time-varying Lawrencian. This is perhaps the most useful diagnostic tool, as the sweeping mode is unmistakable from other modes (due to its distinct motion to-and-fro) and can be used as visual feedback whilst adjusting any parameter affecting the slave laser.

Absorption Spectroscopy The output of the slave is directed through a Rb vapor cell while it is being injected by a sweeping* master. A photodiode placed in the beam path after the cell can distinguish spectroscopic absorption features if the slave is on color.

All of the above checks are good signs of injection locking, but there is no way (known to myself or anyone in the lab) of testing for the presence of power in other optical modes. Fortunately, it seems that a MOT is relatively insensitive to this and will "work"(used loosely) under marginal conditions.

Dual Injection Attempts

Before resorting to the current technique of mixing the master repump light directly into the cooling beam, we had made several attempts at dual-injecting the slave laser. In other words, we attempted to amplify both cooling and repump frequencies at the same time, in the same laser. This process involves mixing the two master beams together before injection, in hopes that the gain medium will allow two frequencies to be amplified simultaneously.

As of yet, we have not been able to confirm whether dual injection has been achieved or even whether it is possible. The output of the slave while being dual-injected was sent into a Fabry-Perot diagnostic cavity for analysis, but no conclusive results were obtained–due in part to the presence of other modes in the power spectrum, as well as the physical difficulty of identifying the correct sweeping modes.

The dual injection attempts were put on the backburner for two reasons. One, as stated above, our diagnostic tools were not entirely conclusive. By far the most conclusive method of testing for the presence of the two amplified frequencies is to observe trapping. At that stage, not only had we not

achieved trapping yet, but the master lasers were not in a state where it was possible to lock both cooling and repump simultaneously. Both frequencies could be produced, but only by sweeping across the repump transition, not locking to it. Hence, we opted to go the more well-traveled route for the time being and only amplify the cooling beam.

Injection Power Test

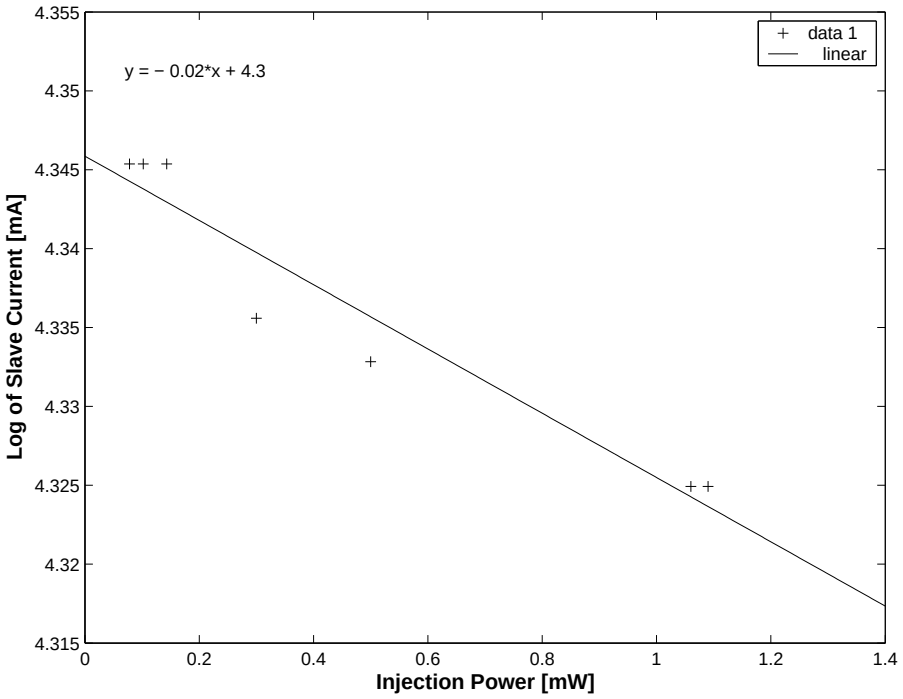

Figure 3.4: A semilog plot of the slave current vs. injection power. Also shown is a linear fit, indicating a roughly decaying exponential relationship between current and injection power. Unfortunately, I have no theoretical model on which to base the measurement.

Throughout the course of aligning MOT optics and waiting for the master lasers' lock system to be repaired, I tested the lowest power at which I could successfully inject a slave laser. Dr. Madison suggested the test to establish a standard to which other injection locks can be compared. Optimally, a slave would be injected with very low power and it would remain injected over a wide bandwidth. Hence, the goal of the test is to inject

throughout the widest bandwidth while using the least power.
The test was conducted as follows. Light from the "Brunette" master laser was passed through a variable attenuator mounted on a translation stage. The master is set to sweep across the Doppler-broadened ^{87}Rb cooling transition so that it is easily visible on the Fabry-Perot trace. Starting with `*perfect*` injection (perfect defined by the limit of our diagnostic tools), a series of incremental decreases in injection power were made, each to the limit of losing roughly half the Fabry-Perot signal from the correct mode. Each time the injection power was decreased, both the injection alignment and the current to the slave were re-optimized to re-establish perfect injection.

Results
Seven trials were performed, each with very successful results obtained by realigning the injection angle and re-optimizing the current to the slave. It is not clear whether the re-aligning was required due to fundamental reasons within the laser diode or whether it was an optical abberation from the variable attenuator. In either case, a notable trend in the slave's current was recorded as the injection power was lowered, see figure 3.4.
As seen in figure 3.4, the lowest injection power achieved was 7.8μW. The test confirms that injection is possible at far lower powers than have been commonly used in the lab. Before this test, it was not uncommon to use several mW of power for injection. The benefit of reducing the injection power is optimizing the effectiveness of the slave as an amplifier, as well as the conservation of optical power.

3.2.2 Design of physical layout

The MAT experiment has three physical sections. The slave amplifier and AOM double-pass occupy one corner of an optical table, the saturated absorption diagnostic occupies the central region between the amplifier and the MOT optics, and finally the MOT optics and vacuum system occupy the corner opposite to the amplifier.
The optical arrangement of the MOT was chosen so as to minimize the number of components. Since Dr. Booth had two large beam-splitting plates in his possession, these were used to split the expanded MOT beams into their three axes. The plates were mounted with epoxy onto the sides of 1" optical mirror mounts so that they could be used to accurately reflect light up to the elevated 7.5" MOT optics, as opposed to splitting the beams and then using separate mirrors for adjustments.

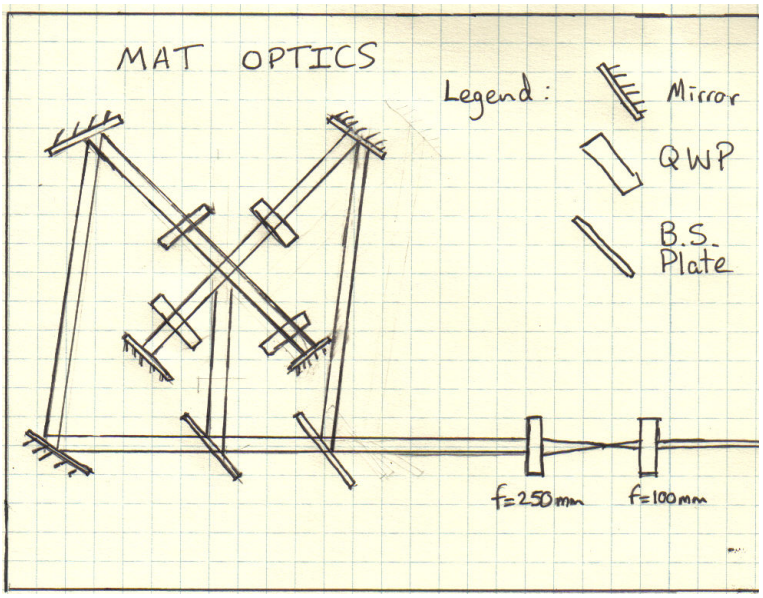

Figure 3.5: A schematic of the MAT optics. The beamsplitting plates caused an etalon effect in the trapping beams, resulting in strange and unique MOT cloud shapes as fine adjustments were made (see results section). The vertical axis is not shown but is fundamentally the same as the other two axes except for the circular polarization helicity is opposite.

3.2.3 Magnetic coils

The present working MOT uses a small pair of coils that existed before the MAT project began. They each have 15 windings and produce a specific gradient of 2.5 G/(cm A), up to a flexible limit of around 11 amps, at which point the equilibrium temperature rises above 70°C, as measured by a thermocouple probe.

For the future of the MAT experiment, a new pair of coils is needed to satisfy higher gradient requirements and the stringent geometry of a mirror MOT*. The physics of the mirror MOT requires the magnetic coil axis to lie parallel with one of the horizontal laser beams; 45° with respect to the inherent mirror. This presents a physical constraint on the size of the coils, as the inner radius must not intersect with the vacuum cell itself, which protrudes from the coils at an angle of 45°. Mathematically, the constraint

can be expressed as[1]

$$ID > 2H + 6t + L + \frac{4w}{\sqrt{2}} \tag{3.3}$$

Where ID is the inner diameter of the coil housing, H is height of the coil windings, t is the thickness of the coil housing, L is the length of the coil windings, and w is the width of the glass cell. For the chosen design, H = 14mm, t = $\frac{1}{16}$" = 1.5875mm, L = 11mm, and the cell width w = 12.5mm. Evaluating the above formula, we have

$$ID > 84mm \tag{3.4}$$

For this reason, an inner diameter of 89mm was selected so as to have a small amount of clearance between the coil and the cell while still maximizing the gradient field. Here are the (untested) specifications of the mirror MAT coils:

Inner Radius	89 mm
Average Radius	52.5 mm
Winding width	14 mm
Winding height	11 mm
Number of Windings	140
Specific Gradient	5.67 G/Acm
Wire gauge	18
Wire diameter	1.02 mm
Resistance per coil	1.95 Ω

The mirror MAT coils are each made from three pieces of aluminum. A short length of machined pipe acts as a cylindrical frame about which the wires are wound, while two thin, annular sheets are fixed to the sides of the pipe with 2-ton epoxy. The thin sheets include four 1/4"-20 size clear holes for mounting either in mirror MOT fashion or vertically for a conventional MOT. In between the mounting holes, the sheets are cut down radially to aid with cooling and for ease of winding.

3.3 Results

On the evening of December 12th, 2006, the MAT began cooling ^{87}Rb atoms to ultra-cold temperatures on the order of 100 μK. Since that date, Dr. Booth and I recorded several measurements characterizing loading rates under varying conditions, as well as a few attempts at magnetic trapping.

The light from the MOT cloud has been imaged onto the surface of a photodiode using a 25mm lens. The signal is measured on a digital oscilloscope with a large time scale, then saved to a floppy disk. When measuring the MOT signal, one must be careful to separate background light noise and electronic noise from the signal. The background light noise has two sources: ambient light and scattered laser light from the cell. The former can be minimized by shutting off all other sources of light, however the latter is something which must be subtracted from the signal.

To observe the MOT loading, the master injection light may be blocked

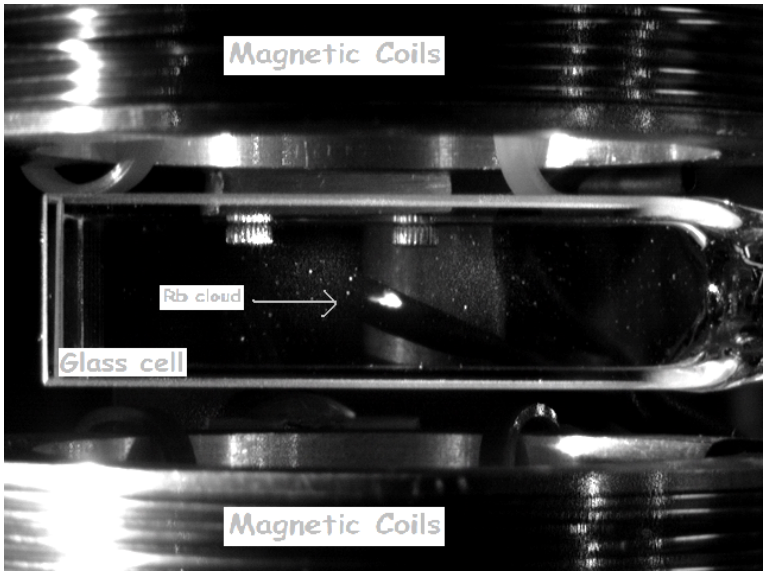

Figure 3.6: An annotated picture of the MAT experiment in operation. Visible are the magnetic coils, the glass UHV cell, and the atomic cloud, which is saturating the CCD detector.

briefly. This way all the scattered light is still being measured, but the slave runs freely and hence does not interact with the atoms, and no MOT exists. Once the injection light is let back in, the MOT begins to load from zero atoms to its equilibrium number, according to the simple rate model[1]

$$\frac{dn}{dt} = R - \frac{n}{\tau} \tag{3.5}$$

whose solution is $n(t) = \tau R\left(1 - e^{\frac{-t}{\tau}}\right)$, where R is the loading rate, n is the number of trapped atoms, and τ is the time constant. In this case

it is assumed that there are not enough atoms to cause nonlinear effects such as collisional losses. When relating this model with the photodiode measurements (assuming a linear correlation between trapped atoms and fluorescence signal), one may take the voltage to be[1]

$$V = V_b + [V_{max} - V_b] \left\{ 1 - exp\left(\frac{t - t_o}{\tau} \right) \right\} \tag{3.6}$$

Where V_b is the background signal, V_{max} is the signal when the trap is

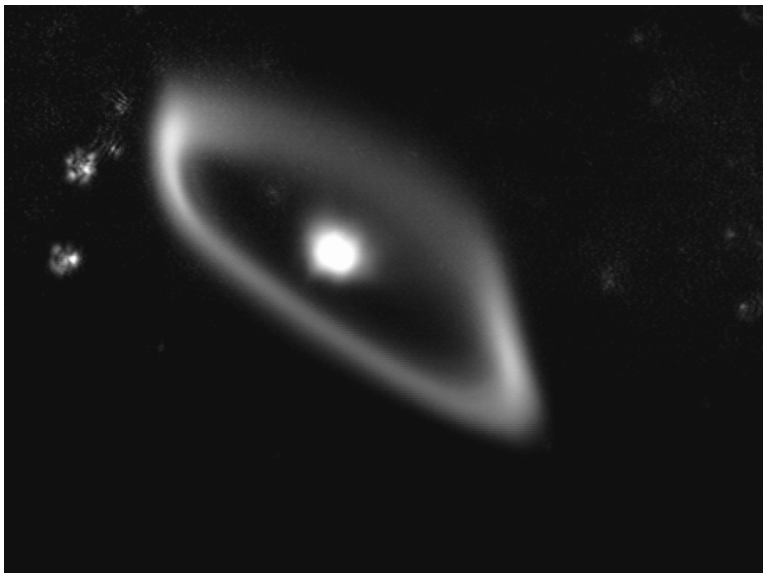

Figure 3.7: A ring-shaped MOT, likely caused by spatial variations in the laser beam intensities. The beam splitting optics consisted of flat plates, which suffer from etalon effects–introducing interference fringes in each beam.

fully loaded, and τ the loading rate time constant; a function of both the overall background pressure and the rubidium partial pressure.
The primary variable of interest affecting loading rate measurements is the Rb dispenser. The device operates by resistive heating, ejecting more and more hot atoms the longer it remains on. Several measurements were made after the dispenser was on for different amounts of time. The data was then fit with an exponential model and the results plotted. The following data was taken on December 15^{th}, after a night of ion pump evacuation and no dispensing. The source was then turned on at 4.75A for 20 minutes, and the

measurement repeated (both cases are shown in figure 3.8).
Additionally, we tested the effect of applying UV radiation as a means of de-sorbing Rb atoms from the cell walls. The high-energy UV photons from a blue-violet LED are able to break the binding energy of the Rb against the glass wall, rapidly increasing the vapor pressure inside the cell. The UV LED was mounted on a post, overlooking as large a portion of the cell as possible, bathing it relatively uniformly in light. It was also necessary to apply a UV filter to the photodiode in order to eliminate any UV from affecting measurements.

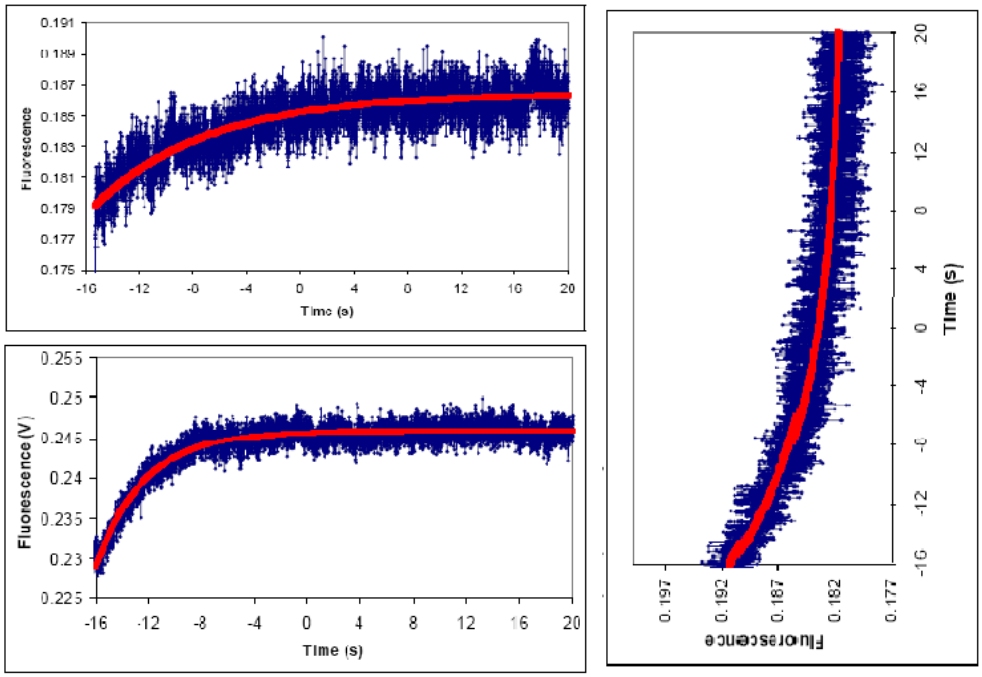

Figure 3.8: [1]Three different fluorescence measurements from the $^{8}7$ MOT. The top is the first loading signal after a night's ion pump evacuation. The lower trace is after turning on the dispenser for 20 minutes at 4.75 A, showing brighter signal and a shorter time constant, as expected. The third (vertical) trace shows the effect of turning on the UV light, allowing equilibrium to come, and then suddenly shutting it off. As predicted, the equilibrium number of atoms is significantly higher when the UV light is applied.

3.4 Discussion

The immediate goals of the MAT experiment will be to measure the stability of the vacuum pressure over time, with and without an ion pump running[1]. Again, the purpose of this test is to attempt to liberate the trapping system from bulky and expensive items such as the ion pump. Since testing vacuum conditions is done most effectively by measuring the rate of loss from a magnetic trap, it shall be the next step to automate such measurements. In the last few days of December, Dr. Booth and I were able to make very rough preliminary measurements of magnetic trapping by doing as follows:

1. Produce a large MOT by running the dispenser for several tens of minutes with a current of 5 amps
2. Increase the magnetic field gradient to the highest possible level, given the magnetic coils' ability
3. Record the equilibrium level of fluorescence
4. Record the level of fluorescence while blocking the master injection light to the slave laser, such that optical power still scatters from the trapping cell but there are no trapped atoms
5. Allow the MOT to re-form, up to equilibrium level
6. Chop the injection beam once more, as rapidly as possible
7. Record the scope trace resulting from the 'full' MOT suddenly losing the effect of radiation pressure and then regaining it after losing a large portion of its atoms from background gas collisions and spin flip losses

The relevant number to record is the fluorescence level immediately after the correct frequency is re-established. This signal represents the number of atoms that remained in the trapping region throughout the 'period of darkness', ie. the trap's loading curve starts from a non-zero value. An important detail to note is that during the time when the atoms are confined by purely magnetic forces, they are in fact there despite our lack of ability to detect them. This is the reason why the fluorescence level must be recorded while blocking the injection beam beforehand, because it represents the signal level that should be observed while the atoms are magnetically confined. Since these initial measurements were performed in a rather rudimentary fashion, they will be repeated in the near future by automating the beam-block and measurement processes such that it can be known exactly for how

long the atoms are magnetically trapped, and this amount can be varied systematically.

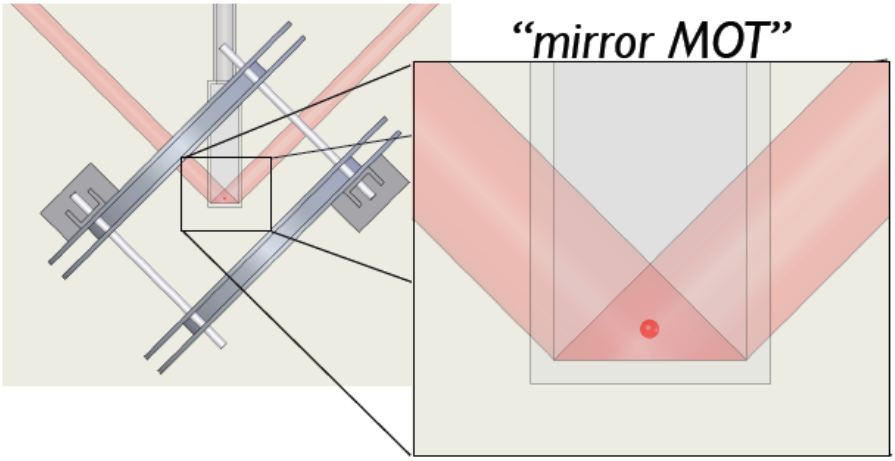

Figure 3.9: A Solidworks image of the proposed Mirror MOT. Not shown is the vertical beam which is identical to that of a conventional MOT. The distance between the inner radius of the coil on the upper left and the vacuum cell is the tightest constraint.

With the presence of a working MOT, the concept of dual injection can now be revisited. However the next attempt will not be identical to the first–previously it was ^{87}Rb cooling and repump to be amplified simultaneously, but it may be easier and more interesting to dual inject the cooling transitions for both ^{87}Rb and ^{85}Rb as they are closer to each other in frequency. In principle, a two species MOT could be made by amplifying both cooling transitions while separately mixing both repump beams. The idea is that since the cooling transitions are spectrally closer in frequency, the gain medium will more easily amplify both at once.
Although the presently functional MOT has been a pleasure to build and observe, this is only the initial stage of the MAT experiment. After more vacuum and dual injection measurements are taken, it will be modified to operate as a mirror MOT, eventually using an anodically-bonded silicon chip to seal the back end of the cell and provide a reflecting surface above which the MOT will form. It is this configuration which will eventually allow the creation of highly-sensitive ”atom chip” sensors.

Chapter 4

Feshbach Experiment

The Feshbach experiment is a test bed for triple species ultra cold collisions and molecule formation. It is the primary focus of the QDG lab to observe heteronuclear electromagnetic feshbach resonances between all possible combinations of ^{6}Li, ^{87}Rb, and ^{85}Rb, as well as perform optical lattice experiments in the same trap. The scope of my contributions to this experiment is the mechanical and magnetic field design of the main chamber; a long, straight vacuum cell with UHV pumps and atom dispensers on one side and high voltage electrodes on the other. This chapter is a short summary of those components I designed before working on the MAT experiment.

4.1 Solidworks models

I have produced Solidworks models of the trapping chamber, vacuum pumps, magnetic coils, support structure, and immediately surrounding optics of the feshbach experiment. The sketch provides a means of visualizing the 3D nature of the experiment, and is a very useful design tool for a system where optical access is essential. All the 2D Solidwork sketches may be found in the Appendix, and include three pairs of earth-field compensation coil frames, a mounting bracket system for the former, an assembled view of the 80/20 support structure with the compensation coils, and the high voltage Feshbach electrodes.

4.1.1 Compensation/Gradient coil design

The compensation coils are three large pairs of rectangular coils, encompassing the entire trapping region. Their primary function is to null the earth's magnetic field, however they are capable of much more than this. Each coil can be driven independently, and as pair can produce uniform field of several Gauss.

The three coil pairs are designed to mount onto a rigid aluminum frame constructed from 80/20 hardware. The coils are mounted on the frame such that all outside corners are still available for mounting optical components,

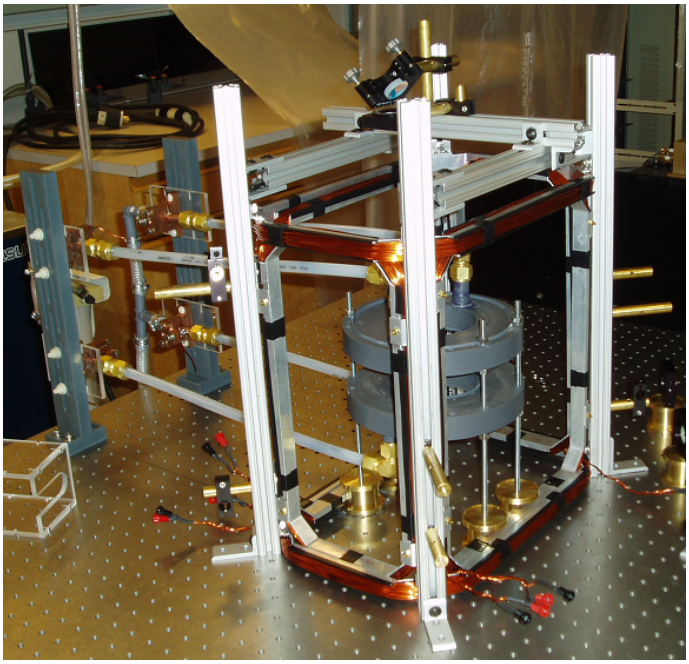

Figure 4.1: The magnetic field hardware for the Feshbach experiment. The water cooled Feshbach coils are supported by four threaded rods, entirely contained within the volume of the compensation coils. Electrical connections for the compensation coils can be seen at the bottom of the image, whereas the Feshbach coils are powered by large connectors located at the water/electrical support structure on the left.

and the coils occupy a minimal amount of useful angle from the trap center, such that laser beams may be shone in from nearly all directions. In particular, the lower sections which run horizontally are designed to sit only 0.25" from the optical table and are only 0.75" tall, giving a clearance of 1" as measured from the table. This is crucial to all the laser beams which propagate at a standard height of 2.5" and are 1" in diameter. Hence there will be a 1" gap between the bottom of all laser beams and the top of the coil frame.
The compensation coil frames were made by the professional machine shop from modified u-channel. The material was cut and then bent into a rectangular shape with 45° corners, to increase the bend radius of the magnet wires. One weld is required to join the two ends where the material was

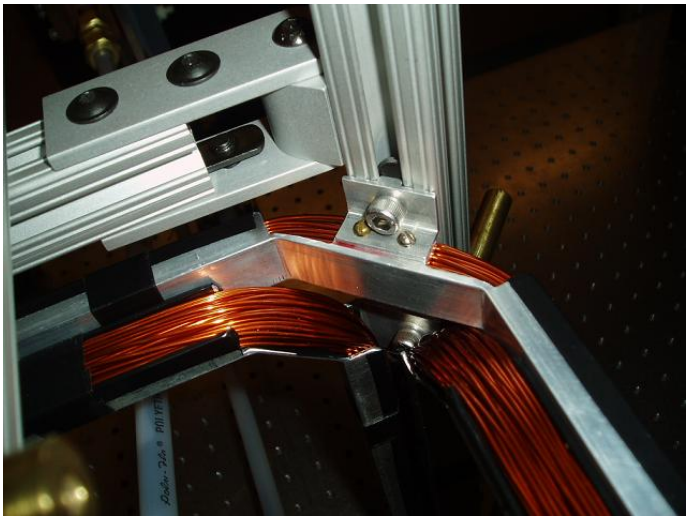

Figure 4.2: The intersection of three compensation coils at a corner. All the coils mount to an 80/20 structure which supports optical components surrounding the experiment.

cut. Each coil frame is mounted independently (and hence independently removable) by four small brackets designed to slide up and down the t-slot feature of the 80/20.

4.1.2 High Voltage Electrode design

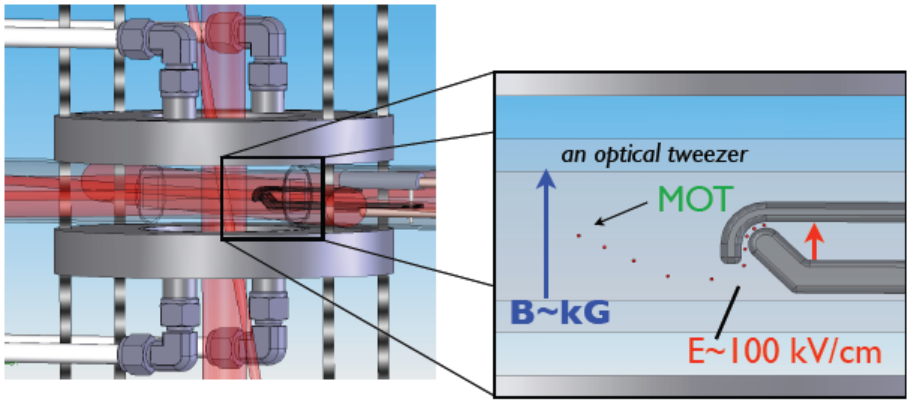

Figure 4.3: A Solidworks screenshot of the high voltage Feshbach electrodes

Chapter 5

Slow Atom Source Design

The slow atom source project originated during discussions with Dr. Kirk Madison in the spring of this year. It had started as a plan to produce a continuous BEC by coupling the output of a two dimensional MOT into a magnetic waveguide. The waveguide would serve as a medium to propagate the cold atoms in beam form, while using RF-induced evaporation methods to further cool them to degeneracy. Had we succeeded, it would have been the first of its kind and of great interest to the atom optics research community.
After a literature search on the topic, it became clear that there were several technical challenges faced by other groups[9] which would prevent it from being a reasonable goal for an 8 month coop project, given the time and resources available. At this point the project evolved into a cold atom beam source, proposed by Dr. Madison, as a means of upgrading the lab's conventional atom dispensers. It would be a modular device, providing a high flux of slow-moving atoms [1] to other more complex experiments which require extremely good vacuum conditions. The beam source would help maintain the vacuum integrity by delivering the slow-moving (and therefore capturable) atoms directly into the trapping region, where they do not add to the background pressure. This is in contrast to less efficient sources, such as ovens, which allow a large flux of atoms to enter the entire chamber where they are captured from their random diffusive motion.

5.1 Literature Review

The first several weeks of the summer were spent doing a literature review. The purpose of the review was to investigate the pros and cons of all the different methods of building a source of cold atoms. We were concerned with the following criteria:

[1] Slower than the capture velocity of a MOT

Property	**Description**
Atomic flux [$atoms/s$]	Higher flux rates not only decrease the amount of time to load a certain number of atoms, but also increase the total number of captured atoms. At least $10^8 atoms/s$ is desirable. [2]
Beam divergence [mrad]	Limiting the beam divergence allows one to capture a larger fraction of the atomic beam from a given distance, for purely geometric reasons. A typical divergence is between $10mrad$ and $50mrad$.
Beam velocity [m/s]	The beam velocity should in general be as slow as possible to ensure a large fraction of atoms in the beam are below the capture velocity of the MOT. However in some cases a minimum value is required to overcome the effect of gravity during ballistic flight from the source to the capture MOT. Beam velocities of a few m/s are achievable with optical cooling techniques.
Required laser power [mW]	This quantity should be minimized such that it can be used elsewhere in the lab. Ideally only one slave laser amplifier producing 30mW of optical power would be needed.
Overall simplicity	Due to time and resource constraints, ease of construction is an important factor. Since placing equipment inside the vacuum is both difficult and potentially compromising, we attempted to minimize if not eliminate this obstacle.
Ability to toggle on/off	With this capability, one could load a trap and then shut off the source so as to not bombard the cooled atoms.

The search turned up two general types of sources: 2D MOTs using laser cooling, and the use of magnetic guides. Laser cooling can produce very high fluxes because it enables you to capture a wider range of the Maxwell-

Boltzmann velocity distribution, as it a selectively applies a slowing force to those atoms moving quickly. The alternative is to use a magnetic guide as a low pass velocity filter, where only those atoms having a low enough velocity will be guided around a curved tube and onwards into the experiment chamber. The advantage of this technique is simplicity of design and versatility. Once such a magnetic guide is built, it can be transferred from one experiment to another, without being constrained by optical alignment. In order to make some qualitative design decisions, information was gathered on six different slow atomic sources, built by four different research groups:

1. A 2D MOT, Universiteit van Amsterdam [4]
2. A 2D + MOT, Universiteit van Amsterdam [4]
3. A Low Velocity Intense Source (LVIS), Universiteit van Amsterdam [4]
4. 2D MOT, Universitat Stuttgart [14]
5. An 'Atom Faucet', Ecole Normale Superieur []
6. A Laser-free slow atom source ('The Skimmer'), Rice University [5]

The group from Universiteit van Amsterdam, whose main author is Kai Dieckmann, conducted a quantitative test by building three sources in the same chamber. All of their sources use optical cooling methods, but in slightly different fashions. As shown in figure 5.1, the 2D MOT is a vapor-loaded trap with only transverse cooling. Atoms from the background vapor pass through the region where the four horizontal beams intersect and are slowed in the transverse directions. Since their original axial velocity remains unaffected, the result is two vertical atomic beams propagating up and down from the center of the chamber. Note that despite the lack of axial cooling, these atomic beams have an average velocity far lower than the thermal velocity of the background gas because only those atoms which are moving slow enough to begin with spend enough time in the molasses region* where they are cooled transversely. The beam traveling upwards passes through a small aperture drilled into the top mirror and into the chamber above, where the pressure is less than 3 x 10^{-11}mbar–more than a factor of 10^4 lower than the pressure inside the source chamber.[3]

[3]The large difference in vacuum pressure is achieved by differential pumping between the source and UHV chamber. This is a common technique in double-MOT systems,

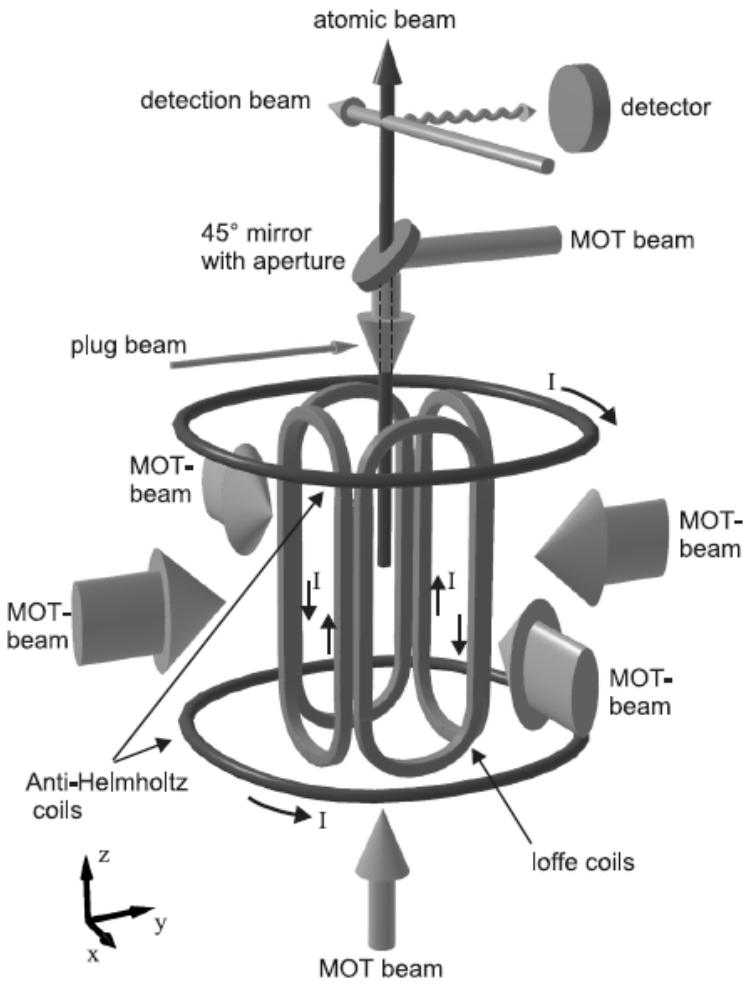

Figure 5.1: [4] A schematic of the three slow atom sources built at Universiteit von Amsterdam. The circular coils produce a spherical quadrupole field (as used in the MAT experiment and most MOTs) for the LVIS, and the elliptical racetrack coils produce the cylindrical quadrupole for the 2D and 2D+ MOTs. In all cases the atoms are extracted through an aperture which provides differential pumping to the chamber above.

The 2D+ MOT is a very close relative to the 2D MOT, the only difference being the addition of laser beams in the axial (vertical) direction. These beams contribute to molasses cooling in the axial direction, but do not provide a confinement force as the magnetic field has a negligible gradient in this direction. They also serve as a means of exerting a net upwards force by varying the relative intensity of the upwards propagating beam versus the downwards propagating beam. The intensities which produced the highest atomic flux were 2.1mW and 0.64mW for upwards and downwards, respectively. The effect of the axial beams nearly doubles the total flux and halves the average axial velocity; a much more efficient source than transverse cooling alone. Here the results of the 2D+ MOT are summarized:

- Atomic flux = 9 x 10^9/s
- Mean velocity = 8 +/- 3.3 m/s
- MOT background pressure = 1.5 x 10^{-7} mbar
- Beam divergance = 43 mrad
- Total laser power = 17.74mW
- Experimental Details: External magnetic coils, elliptical retro-reflected MOT beams, axial cooling beams of asymmetric intensity, and a modified mirror inside the vacuum.

The LVIS source is based on one of the first slow atom sources conceived [11]. It is identical to a vapor cell MOT in all respects except one of its mirrors has a small aperture drilled through it, such that there is a 'shadow' in the center of the cooling beam from that direction. Hence if an atom ventures into the region where the shadow intersects the other beams it will, on average, feel a force towards the aperture. Some atoms will be forced into trajectories direct enough to travel all the way through the aperture, forming an upwards beam which travels into the UHV chamber. The LVIS source was characterized by a high performance at low vapor pressures, but is far less effective than the 2D versions as the pressure approached saturation. It is effective at lower pressures because it exerts three dimensional confinement. Atoms which do not get pushed out into the aperture initially get recycled and generally do not leave the trap until they eventually exit through the aperture[4].

where a vapor-loaded MOT cloud is transported through a differential pumping tube into a second region of higher vacuum quality.

The summarized results of the LVIS:

- Atomic flux = 2 x 10^8/s
- Mean velocity = 26±6.3 m/s
- MOT background pressure = 3 x 10^{-8} mbar
- Beam divergance = 27 mrad
- Total laser power = 19.4mW
- Experimental Details: External magnetic coils, circular retro-reflected MOT beams, axial cooling beams of asymmetric intensity, and a modified mirror inside the vacuum.

These results clearly show that a 2D+ MOT source is an order of magnitude more effective (brighter) than a LVIS, with very similar experimental complexity. For this reason we chose to eliminate the LVIS as a possible design.
For comparison to the 2D and 2D+ MOTs of the Universiteit van Amsterdam, we also considered a **2D MOT source built at Universitat Stuttgart**. This group demonstrated a 2D MOT source in a small cell with no in-vacuum components and no extra push beams or radiation imbalances. They were also able to achieve the highest rate of atomic flux, which lends credit to the transverse cooling technique: it does not suffer from collisional losses, and as a result one may increase the vapor pressure to very high levels before inefficiencies occur. In this case, the Rb vapor pressure was raised a factor of ten above the saturation pressure of 3x10^{-7}mbar by heating the 2D MOT cell with electric heating rods. Correspondingly, their flux was a factor of ten higher than the 2D MOT:

- Atomic flux = 5 x $10^1$0/s
- Mean velocity = 50 m/s
- MOT background pressure = 2 x 10^{-6} mbar
- Beam divergance = 32 mrad
- Total laser power = 320 mW
- Experimental Details: External magnetic coils, circular retro-reflected MOT beams, axial cooling beams of asymmetric intensity, and a modified mirror inside the vacuum.

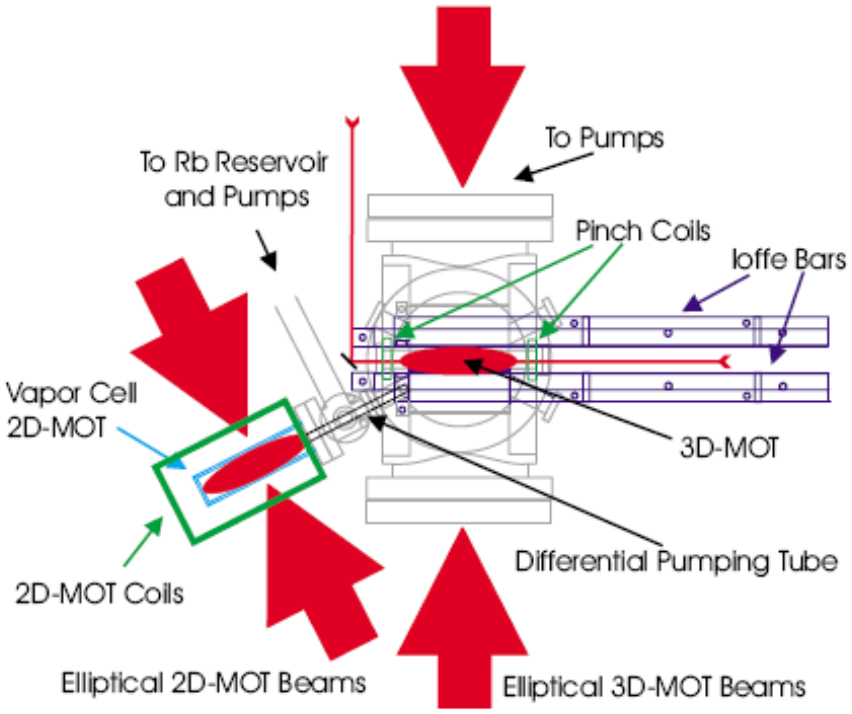

Figure 5.2: [14] A technical drawing of a 2D MOT loading a 3D MOT, built at Universitat Stuttgart. The highly elliptical laser beams help to increase the trapping volume as well as reduce the atomic beam divergence, by creating a high aspect ratio molasses region. Also note the presence of the differential pumping tube connecting the two chambers. This cold atom source is characterized by a very high vapor pressure and as a result, very high atomic flux.

Although simple to construct and very intense, the source relies heavily on copious laser power and high vapor pressure. The group was using a powerful and expensive laser system; a $1.3W$ Titanium-Sapphire laser pumped by a $10W$ Verdi producing $1W$ of usable light at 780nm. With this much power, they were able to use light 20 times the saturation intensity with beam profiles of 95 x $15mm$. With this level of intensity, even the edges of the wide beams exceeded saturation intensity and therefore contributed fully to transverse cooling. Since it was not in the immediate plan to install such a laser system, we would not use the same approach for our cold atom source. Another atomic source making use of molasses cooling is the 'Atom Faucet'. It is quite a nice, simple source consisting of a standard MOT with a push beam and a differential pumping tube. Trapped atoms are forced downwards by the radiation imbalance and out the differential pumping tube. The advantages of this method are ease of construction, low beam velocity, low beam divergence, and excellent vacuum quality on the recapture side:

- Atomic flux = 1.3 x 10^8/s
- Mean velocity = 14 m/s
- MOT background pressure = 2 x 10^{-8} mbar
- Recapture MOT pressure = 10^{-11}mbar
- Beam divergance = 10 mrad
- Total laser power = 60 mW
- Experimental Details: External magnetic coils, circular retro-reflected MOT beams, and a differential pumping tube. No optical components are placed inside the vacuum.

The atom faucet is certainly the simplest of all the above sources and its performance is respectable.

5.2 Magnetic Guiding Theory

The magnetic guide design we considered is quite simple. A small oven housing one or more alkali species in separate compartments would attach to a curved stainless steel tube. The tube, lined with either permanent magnets or conducting wires, would be mounted to a standard 2.75" conflat

flange on the opposite end for the purpose of portability. The wires/magnets produce a DC field whose minimum lies along the guide's axis, such that there is a radially-symmetric gradient always pointing towards the center; see equation 5.4.
The force on the atoms is produced by the Zeeman effect. The Zeeman effect manifests itself as a splitting of hyperfine electron energy levels in the presence of a magnetic field, caused by the energy associated with the electron's magnetic moment projected onto the external field. The ground states of our trapping species ^{6}Li, ^{85}Rb and ^{87}Rb all contain weak field-seeking Zeeman sublevels, meaning they see an increase in potential energy as a function of magnetic field strength. The Zeeman force is then the negative gradient of this potential:

$$\overrightarrow{F} = -\overrightarrow{\nabla}(\phi) = -\mu_b g_F m_F \overrightarrow{\nabla}|\overrightarrow{B}| \tag{5.1}$$

Where μ_b is the Bohr magneton, g_F is the Lande g-factor, and m_F is the quantum number of the magnetic sublevel. If we are to control the motion of atoms from one side of a tube to the other, they must be in this weak field seeking state. Between the two ground states of ^{87}Rb there are three weak field seeking magnetic sublevels (for small fields): $m_F = 1, 2$ for the $F = 2$ ground state and $m_F = -1$ for the $F = 1$ ground state. The state distribution of atoms emerging from an oven-like dispenser can be assumed random[12], and hence only $\frac{3}{8}$ of the atoms are even possible to guide, assuming they remain in a weak field seeking state. Unfortunately, this is not always true!

5.2.1 Majorana spin flips

The Zeeman force is of course dependant on the ability of an atom to remain in its weak field seeking state. Since the state is defined by the orientation of the electron spin with respect to the external field, the atom must constantly re-orient itself while it travels through what it experiences as a changing field. Its ability to do so depends on its Larmor frequency being much greater than the normalized rate of change of magnetic field seen by the atom:

$$\omega_L = \frac{\mu_B m_F g_F B_{loc}}{\hbar} \gg \frac{1}{B_{loc}} \left| \frac{d\vec{B}_{loc}}{dt} \right| \tag{5.2}$$

This is called the Majorana condition [5]. When this condition is not met, the atom undergoes a spin flip into a strong field seeking state and is lost from the guide. One must be careful when applying this condition because it

is the modulus of the *vector* field rate of change that matters, not the rate of change of the modulus. It is not obvious whether the numerical simulations performed in [5] took this into account correctly. It may be that such a mistake is what caused their source's flux to be a factor of 10^3 lower than simulated prediction.
The low-pass velocity filter effect is achieved by introducing a bend into the guide. The force on the atom is limited by the gradient strength, but if the velocity is large enough such that

$$\frac{mv^2}{R} > -\mu_b g_F m_F \overrightarrow{\nabla} |\overrightarrow{B}| \tag{5.3}$$

where R is the bend radius, then the atom collides with the wall of the guide where it either sticks or is repelled in a random direction. This is much more desirable than having a steady flow of high-energy atoms pass directly into the UHV chamber. The velocity cutoff can be tuned by selecting the correct magnetic field gradient and radius of bend. This can also be achieved by using current carrying wires, where one can adjust the gradient by adjusting the current. In this way the cutoff velocity can be selected or even completely shut off, both done electronically and hence very quickly. This is a very important feature that is a distinct advantage over using permanent magnets.
As will be detailed below, a Monte Carlo style Fortran90 simulation, BeamSim, has been written to model the trajectories of individual atoms down the magnetic guide. The simulation hopes to answer whether we can obtain a high enough capturable flux by building a skimmer from a curved tube and magnet wire, or whether we should sacrifice adjustability for higher gradients and use a permanent magnet scheme as was done at Rice University [6] on the original Skimmer. The simulation also models coupling efficiency into a magnetic guide for varying wire geometries.

Four wire quadrupole gradients

The most common way of making a magnetic guide is with a four wire quadrupole, or racetrack coils. In the approximation that you are a large distance from the edge of the guide, it appears as four infinite wires placed on the vertices of a square, with the current direction in each wire the same as its diagonal but opposite from its adjacent. It is essentially a stretched out anti-Helmholtz* coil pair, producing a field whose first order terms are

$$\overrightarrow{B} = b^{'}(x\hat{x} - y\hat{y}) \tag{5.4}$$

where $b^{'}$ is the gradient strength and the guide lies along the z-axis. There is no axial component in the field. As a rough approximation assuming infinite wires and a linearly increasing field,

$$b^{'} = \frac{4\mu_o I}{\pi a^2} \tag{5.5}$$

which is derived from calculating the field on the midpoint between two adjacent wires and dividing by the distance to the center, $\frac{a}{2}$, where a is the side length of the guide.

5.3 MATLAB and Fortran 90 Simulations

A combination of MATLAB and Fortran90 code has been written to characterize the performance of a low pass velocity skimmer. Roughly based on the simulations written by Tao Kong in his Masters' thesis[7], the simulation simply integrates the equations of motion for individual atoms launched down a magnetic guide:

$$\ddot{x} = \frac{1}{m}(-\mu_b g_F m_F \overrightarrow{\nabla}|\overrightarrow{B}| - mg\hat{y}) \tag{5.6}$$

where m is the mass of the atom, the first term is the Zeeman force described in the guiding theory and $-mg$ is the force of gravity.
In order to explore all possibilities in parameter space, each atom is given a random initial position and transverse velocity with gaussian distribution and an initial magnetic sublevel with uniform distribution. A longitudinal 'launch' velocity is also added to the randomized transverse velocity in order to test the performance the guide with varying oven temperatures. The integration is then carried out using the fourth order Runge-Kutta method for discrete time elements. At every time step, the algorithm uses the current position and velocity of the atom. It then calculates the force (and therefore acceleration) based on the atom's position in the magnetic field, and outputs a new position at $t = t + dt$, where dt is the discrete time step.
After the new position is known, the boundary conditions are verified. There are three conditions that may result in an atom being lost from the guide:

1. Boundary collision
2. Background loss
3. Spin flip loss

The boundary collision occurs if the atom happens to wander outside the region defined by the guide tube, and is the most common loss mechanism. The second loss type is a background gas collision–a stochastic process proportional to the pressure in the tube. At every time step, a random variable is called and its value compared to a constant that is proportional to the pressure. The higher the pressure, the more likely there will be a collision at every time step and hence more losses. The final type, spin flip losses, are detailed in section 5.2.1.
The Runge-Kutta method requires the force on the atom at every time step. This force arises from the Zeeman effect as described in 5.2 above, and depends explicitly on the magnetic field gradient. To maximize the accuracy of the simulation, a numerical array of magnetic field values was produced in MATLAB. This way BeamSim.f90 could be applied to any arbitrary current carrying wire configuration. The numerical array is read by BeamSim.f90 and used as a lookup table, with indices calculated from the position of the atom.

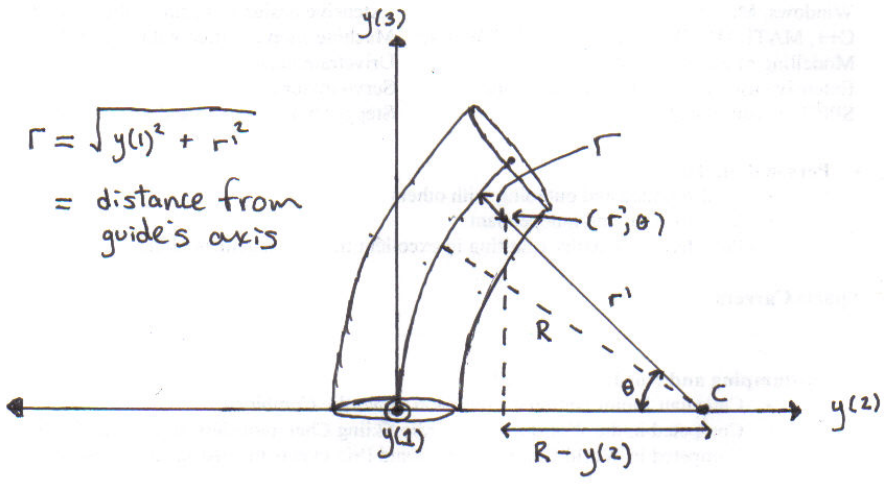

Figure 5.3: The geometric coordinates used in the BeamSim.f90 program. These coordinates were used in order to map an atom's position into the 2D plane which is normal to the guide's axis and coincides with the atom.

$$\theta = tan^{-1}\left\{\frac{y(3)}{R-y(2)}\right\}$$

$$r' = \sqrt{y(1)^2 + (y(2) - R(1-\cos\theta))^2 + (y(3) - R\sin\theta)^2}$$

$$r = \sqrt{y(1)^2 + r'^2}$$

$$i_x = int\{\frac{y(1)+r_o}{\delta_x}\} + 1$$

$$i_y = int\{\frac{\sqrt{r^2-y(1)^2}+r_o}{\delta_y}\} + 1$$

Where i_x and i_y are the indices used for 2D magnetic field lookup, R is the radius of the vacuum tube's bend, r is the distance between the atom and the axis of the guide, $r^{'}$ is the distance between the atom and the guide's center of curvature in the y(2)-y(3) plane, δ_x and δ_y are the gridpoint spacings in the magnetic field array, and $y(i)$ is the atom's cartesian coordinate in the i^{th} direction.
At every time step, the x and y indices for magnetic field lookup were calculated by transforming from 3D cartesian to a 2D cartesian plane that is centered on the guide's axis and coincides with the atom. The magnetic field and its gradient at that location could then be found using a linear interpolation between the four nearest datapoints.

The effect of an Axial Bias Field

Majorana spin flip losses can be greatly reduced by the application of a relatively small bias field along the axis of the guide. The bias has the effect of lifting the minimum to a non-zero value, such that $\frac{1}{B_{loc}}$ does not become arbitrarily large. The effectiveness of the bias field is confirmed by my numerical simulation as well as experimental data from other groups[3]. To apply a bias field, one would wrap a sparse solenoid around the guide, such that when a small current is passed a uniform field will exist along the guide's axis, and the new (approximate) field will be

$$\overrightarrow{B} = b^{'}(x\hat{x} - y\hat{y}) + B_o\hat{z} \tag{5.7}$$

and the magnitude:

$$B = \sqrt{B_o^2 + b'^2(x^2 + y^2)} \tag{5.8}$$

such that there is always a small field B_o present, even if $x = y = 0$.
Once we had established a means of characterizing the guide's efficiency as a function of launch velocity[4], we could begin doing calculations that

[4]The loading rate (and hence equilibrium number of atoms) in a MOT is a strong function of its capture velocity V_c. V_c is the maximum velocity an atom emerging from

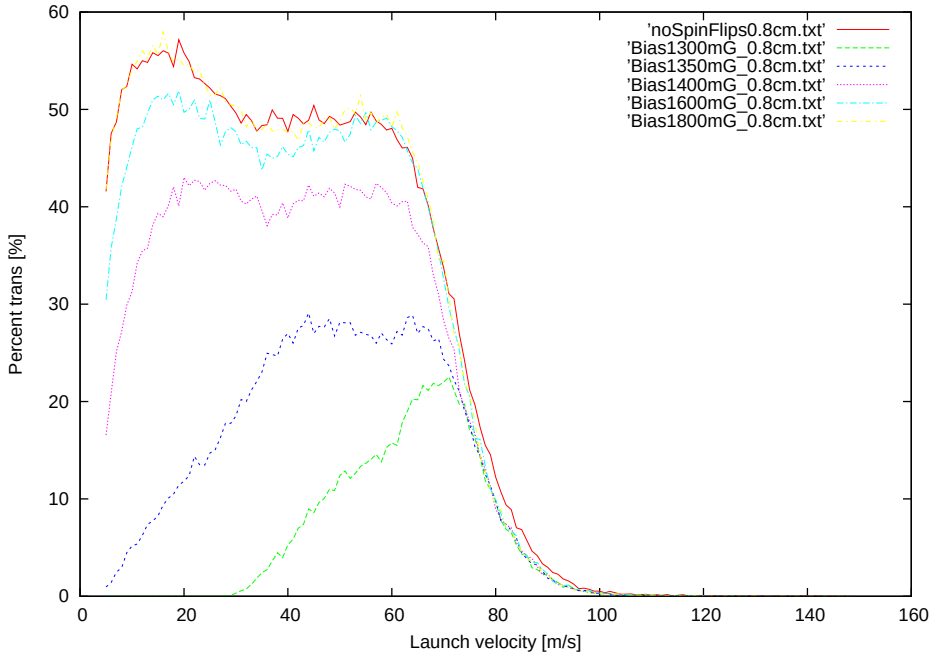

Figure 5.4: The plot shows the fraction of atoms which were guided through the tube successfully as a function of initial velocity. The simulation was completed for several values of bias, ranging between 1.3G and 1.8G. The plot for a 1.8G coincides with that which completely disallowed spin flips, indicating that a rather modest bias will all but eliminate spin flips.

lead towards predicting the total atomic flux that would be guided successfully and subsequently captured by a MOT. Geometric factors aside, the rough calculation is done by multiplying the guide efficiency by a normalized Maxwell-Boltzmann distribution curve for an oven at 300°C. In other words, choose a velocity. Evaluate the magnetic guide efficiency at that velocity, then multiply it by the probability density of an atom emerging from the oven at that velocity. Do this for all velocities and integrate the result from zero to velocity V_c, the capture velocity of the MOT. Finally, plot the integral as a function of V_c.

$$\eta(v) = \int_0^v \alpha(v) f_v = \int_0^v \alpha(v) \left\{ \frac{m}{2\pi kT} \right\}^{\frac{3}{2}} v^2 \exp\left\{ \frac{-mv_z^2}{2kT} \right\} \tag{5.9}$$

the guide can have and still be captured by the MOT.

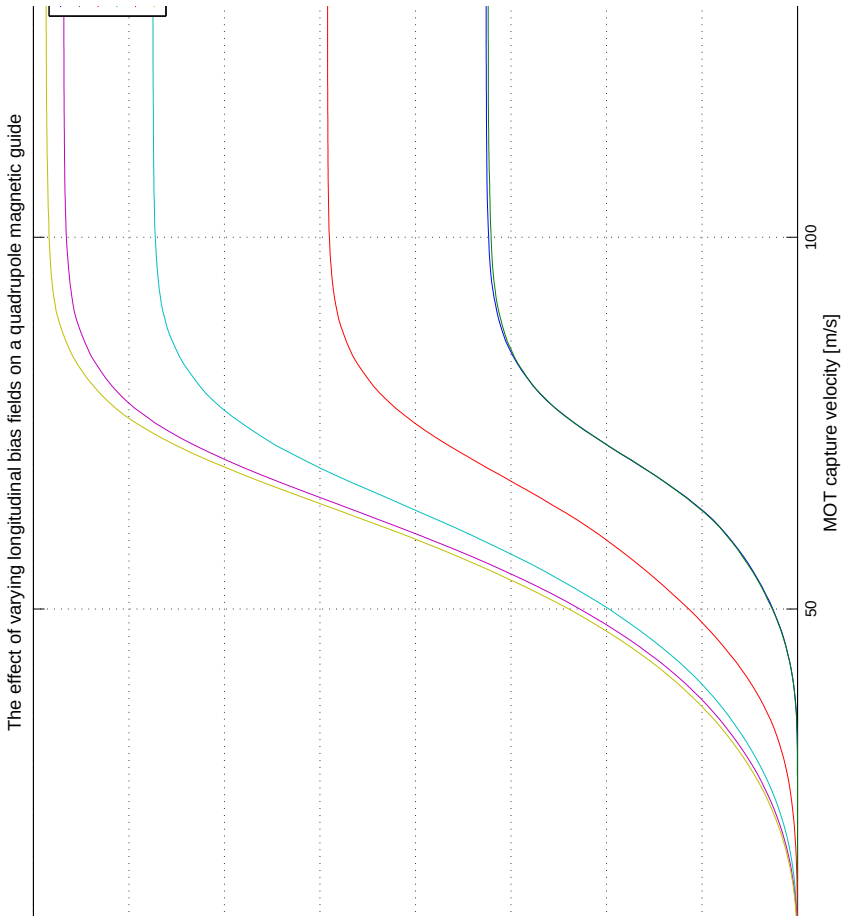

Figure 5.5: Each curve represents the result of magnetic guide efficiency multiplied against the normalized Maxwell-Boltzmann distribution, then integrated over velocity.

Figure 5.5 shows that increasing the MOT capture velocity will lead to an increased fraction of the Maxwell-Boltzmann distribution that is capturable, up to a certain maximum value. At velocities higher than this value, the atoms are not reaching the end of the guide because they are crashing into the walls and not transmitted into the UHV chamber.
One of the most important factors influencing the total atomic flux of a skimmer is either the total trap depth. Depth can be measured in temperature, and represents the total potential energy differential, or the temperature of the hottest 'guidable' atom. The depth can be increased in two ways: increasing the strength of the magnetic field source (by either increasing amp-turns or concentrating the field from permanent magnets) or decreasing the diameter of the guide. The first method is obvious, the second–not quite as much. To illustrate, a quadrupole field has a nearly linear gradient over a large range. The total trap depth can then be made equal to the gradient (a constant) times a, a fixed fractional distance from the guide axis. Despite the trap depth now being proportional to the size of the guide, the gradient strength is proportional to $\frac{1}{a^2}$, increasing the trap depth as the size is decreased.
While attempting to first maximize the gradient strength, we found that permanent magnet gradients were far more powerful than the finite-sized quadrupole magnetic guides running even hundreds of amps. In 'The Skimmer'[5], gradients of 20,000 G/cm were achieved using an octopolar arrangement just outside a metal vacuum tube, as compared with the several hundred that are typical of electromagnetic guides running several hundred amp-turns.
With such high gradients, it would be possible make the diameter larger and still have a large trap depth; capturing far slow atoms from the oven.

Octopolar Fringe Field

As part of the design process, one must predict what sort of effect the field at the end of the magnetic guide will have on a nearby experiment[12]. I calculated the maximum field strength along a radial line as a function of distance from an octopolar magnetic lens. The purpose of this calculation is to verify that installing a magnetic guide in the immediate proximity of a MOT will not have any deleterious effects. The lens is constructed from 8 dipoles placed on the radius of a circle, each having the opposite polarity of its two nearest neighbors. The plot below displays the fringe decay from an octopole lens which produces a gradient of 20,000G/cm within the lens itself. As shown in figure 5.6, the field decays to less than $10^{-3}G$ within

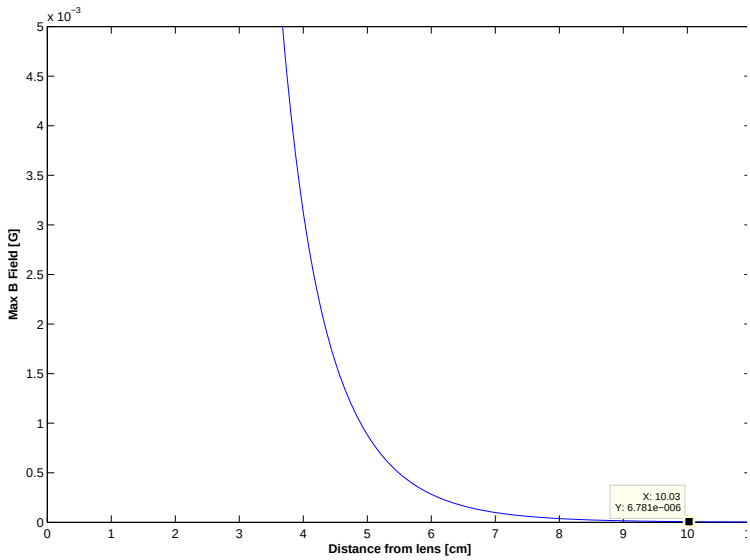

Figure 5.6: A Matlab model of the magnetic field decay as a function of axial distance from a permanent magnet octopolar lens/guide. The field is the same as would be produced by eight small coils placed on the boundary of a tube with radius 6mm, each coil's dipole facing either directly inwards or directly outwards, and the opposite of its immediate neighbor.

5cm, and hence should not interfere with MOT gradients.

5.4 Discussion

It is unfortunate that the state of the cold atom source is still all on paper, so to speak. Throughout the summer I was able to search the literature, brainstorm ideas, and write a numerical simulation in hopes of finding the optimal design parameters for loading the Feshbach and Photoassociation experiments with cold atoms. As the end of the summer approached, my priorities were shifted over to more pressing things such as mechanical and magnetic design for the Feshbach table as well as the MAT experiment. The cold atom source was 'put on the backburner', however I continued to become more involved in the other projects as they progressed, and soon all my time became dedicated to them.

This was partly justified by the fact that a cold atom source is both useless and impossible to test without the existence of a MOT in the first place. For this reason the MAT experiment was an obvious choice for immediate effort, being the most likely to produce a MOT in the short term. After we had a working MOT, I could then theoretically complete the cold atom source and test it out. As it turned out, it was mid-December when the MOT started working and so continuation of the cold atom source was impossible before the end of my eight month work term.
That being said, there is nothing to prevent the source from being built in the future. The device should not be terribly difficult to make, but before construction begins, there are some important calculations to be done:

- Calculate the guide coupling efficiency for a specific oven design
- Multiply the expected oven velocity distribution curve against the guiding efficiency to obtain an expected axial velocity distribution
- Integrate the above prediction to obtain a total predicted atomic flux rate
- Calculate the beam divergence from the end of the guide based on the average transverse velocity of the atoms

These calculations can be done using the BeamSim program, with perhaps a few modifications. Another thing which could be done is to simulate the effectiveness of a small electromagnetic switch on a permanent magnet guide. The idea is to introduce a small perturbation that would be enough to cause the large majority of atoms to crash into the guide's wall. In this way one could toggle the source on/off by turning on the switch coil. It would be very valuable to gain the benefit of an electromagnetic guide while utilizing the gradient strength of permanent magnets.

Bibliography

[1] J.Booth, personal communication, September-December 2006

[2] J.Booth, "Saturated Absorption Spectroscopy: Review", (unpublished) 2006

[3] P. Cren, C.F. Roos, A. Aclan, J. Dalibard, and D.Guery-Odelin, Eur. Phys. J. D 20, 107 (2002)

[4] Kai Dieckmann, "Bose-Einstein Condensation with High Atom Number in a Deep Magnetic Trap" (PhD Dissertation, Universiteit van Amsterdam, 2001)

[5] Jordan Mitchell Gerton, "Laserless Slow Atom Source for Loading Atom Traps" (Master of Arts, Rice University), 1997

[6] B. Ghaffari, J. M. Gerton, W. I. McAlexander, K. E.Strecker, D.M.Homan, and R. G. Hulet, Physical Review A Vol.60(5)

[7] T.Kong, "Progress towards the Study of Li+Rb Ultra-cold Collisions",(Masters' thesis, University of British Columbia) 2005

[8] T. Lahaye, J.M. Vogels, K. J. Gnter, Z.Wang, J.Dalibard, and D. Gury-Odelin, Phys. Rev. Lett. 93, 093003 (2004)

[9] T. Lahaye, Z. Wang, G. Reinaudi, S. P. Rath, J. Dalibard, and D.Gury-Odelin, Phys. Rev. A 72, 033411 (2005)

[10] P.Lebel, "Contributions to the UBC Quantum Degenerate Gas Lab: January-May 2005", 2005 (unpublished)

[11] Z. T. Lu, K. L. Corwin, M. J. Renn, M. H. Anderson, E. A. Cor-

nell, and C. E. Wieman. Phys. Rev. Lett., 77:3331, 1996.

[12]K.Madison, personal communication, May-December 2006

[13] QDG Lab Internal site, URL: "www.physics.ubc.ca/ qdg/internal", (accessed December 2006)

[14] Volker Schweikhard, "Ultracold Atoms in a Far Detuned Optical Lattice" (PhD Dissertation, Universitat Stuttgart, 2001)

[15] V. Vuletic, T. Fischer, M. Praeger, T. W. Hnsch, and C. Zimmermann, Physical Review Letters vol.80, No. 8 (1998)

[16] W. Wohlleben, F. Chevy, K. Madison, and J. Dalibard, Eur. Phys.J. D 15, 237244 (2001)

Appendix A

Solidworks Sketches

Appendix B

Sample Numerical Simulation output